Faculty of Engineering Science
Department of Mechanical Engineering
Control theory [H04X3a]

Report Assignment 4: Control of a pendulum

Academic year 2021 – 2022

Matthias Derez, Toon Servaes

Contents

List of Figures

List of Tables

1 Modeling and Identification of the System

1.1 Theoretical continuous Model

The configuration of the pendulum placed on the cart is depicted in Figure 1, along with the definition of the position of the cart x and the angle of the pendulum θ. In Figure 2, the free body diagram of the pendulum is shown. The pendulum is depicted as a mass m, placed in the center of gravity of the the real pendulum. This mass is connected to the rotation point via a massless bar with length L. This way, the moment of inertia J can easily be computed:

$$J = m \cdot L^2 \tag{1}$$

To derive the continuous model of the velocity-steered cart with pendulum, Newton's second law of motion for rotation is used. There are three contributions to the total moment working on the pendulum system. These are caused by gravity, damping and an inertial force because the pendulum is placed in an accelerating reference frame. These can be filled in into Newton's second law:

$$J\ddot{\theta} = -mgL\sin(\theta) - m\ddot{x}L\cos(\theta) - c\dot{\theta} \tag{2}$$

Using Equation 1, this can be simplified to:

$$L\ddot{\theta} + \ddot{x}\cos(\theta) = -g\sin(\theta) - \frac{c}{mL}\dot{\theta} \tag{3}$$

The parameters of the theoretical continuous model of the velocity-steered cart are x and θ. The input is the cart velocity $\dot{x}$ which has units $[m/s]$. The outputs of the model are the cart position x with units $[m]$ and the pendulum angle θ with units $[rad]$.
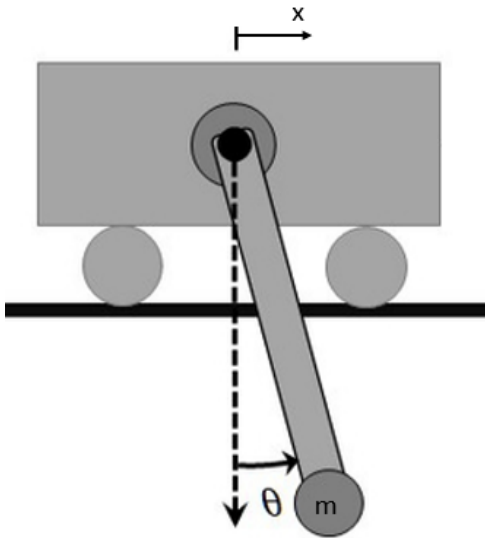

Figure 1: Depiction of the pendulum placed on the cart [4]
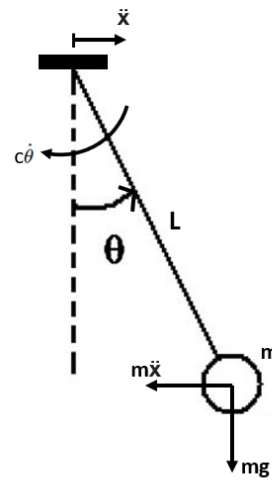
Figure 2: Free body diagram of the pendulum [2]

1.2 State-space Equation for the non-linear Model

To derive a state-space equation for the non-linear model, following states are used:

$$\xi = [x, \theta, L\dot{\theta} + \dot{x}\cos(\theta)]^T \tag{4}$$

In this state vector, x stands for the position of the cart and θ stands for the pendulum angle. In the third state $L\dot{\theta} + \dot{x}\cos(\theta)$, the tangential velocity of the centre of gravity of the pendulum with relation

to a standstill reference frame can be recognized. For this reason, we will call the third state v_{tan} from now on. The state vector then becomes:

$$\xi = [x, \theta, v_{tan}]^T \tag{5}$$

Using Equation 3 and the definition of ξ, the nonlinear state-space equation can be derived. The input is the velocity of the cart and is denoted as v_c.

$$\dot{\xi} = \mathbf{f}(\xi, v_c) = \begin{bmatrix} \dot{x} \\ \dot{\theta} \\ L\ddot{\theta} + \ddot{x}\cos(\theta) - \dot{x}\sin(\theta)\dot{\theta} \end{bmatrix} = \begin{bmatrix} v_c \\ \frac{v_{tan} - v_c\cos(\theta)}{L} \\ -g\sin(\theta) - (\frac{c}{mL} + v_c\sin(\theta))(\frac{v_{tan} - v_c\cos(\theta)}{L}) \end{bmatrix} \tag{6}$$

$$\mathbf{y} = \begin{bmatrix} x \\ \theta \end{bmatrix} = \begin{bmatrix} 1 & 0 & 0 \\ 0 & 1 & 0 \end{bmatrix} \xi + 0 \cdot v_c \tag{7}$$

1.3 Linearization of the Model

The nonlinear model can be linearized around the equilibrium state $\xi_0 = [0, 0, 0]^T$. Both θ and v_{tan} have to be zero in the equilibrium state. The value of x doesn't really matter, but is taken equal to zero for convenience. The equilibrium input v_{c0} is also chosen to be equal to zero. Calculating the jacobian matrices $\mathbf{F}$ and $\mathbf{G}$, we can rewrite the model as:

$$\delta\dot{\xi} = \mathbf{F}\delta\xi + \mathbf{G}\delta v_c \tag{8}$$

Where $\delta\xi$ and δv_c are defined as follows:

$$\delta\xi = \xi - \xi_0 = \xi$$
$$\delta v_c = v_c - v_{c0} = v_c \tag{9}$$

Using nonlinear Equation 6, $\mathbf{F}$ and $\mathbf{G}$ are defined as:

$$\mathbf{F} = \frac{\partial \mathbf{f}}{\partial \xi}\bigg|_{\xi_0, v_{c0}}$$
$$\mathbf{G} = \frac{\partial \mathbf{f}}{\partial v_c}\bigg|_{\xi_0, v_{c0}} \tag{10}$$

From Equation 10, the following matrices arise:

$$\mathbf{F} = \begin{bmatrix} 0 & 0 & 0 \\ 0 & 0 & \frac{1}{L} \\ 0 & -g & \frac{-c}{mL^2} \end{bmatrix} \tag{11}$$

$$\mathbf{G} = \begin{bmatrix} 1 \\ \frac{-1}{L} \\ \frac{c}{mL^2} \end{bmatrix}$$

As the measurement equation was already linear, we find the following linear state-space model:

$$\delta\dot{\xi} = \begin{bmatrix} 0 & 0 & 0 \\ 0 & 0 & \frac{1}{L} \\ 0 & -g & \frac{-c}{mL^2} \end{bmatrix} \delta\xi + \begin{bmatrix} 1 \\ \frac{-1}{L} \\ \frac{c}{mL^2} \end{bmatrix} \delta v_c \tag{12}$$

$$\mathbf{y} = \begin{bmatrix} x \\ \theta \end{bmatrix} = \begin{bmatrix} 1 & 0 & 0 \\ 0 & 1 & 0 \end{bmatrix} \xi + 0 \cdot v_c \tag{13}$$

By applying the laplace transformation to Equation 12, following transfer functions can be found.

$$\frac{d\delta x}{dt} = v_c \rightarrow H_x(s) = \frac{\delta X(s)}{\delta V_c(s)} = \frac{1}{s}$$

$$\frac{d\delta\theta}{dt} = \frac{v_{tan} - v_c}{L} \rightarrow H_\theta(s) = \frac{\delta\Theta(s)}{\delta V_c(s)} = \frac{-1}{sL} \tag{14}$$

$$\frac{d\delta v_{tan}}{dt} = -g\delta\theta - \frac{c}{mL^2}\delta v_{tan} + \frac{c}{mL^2}\delta v_c \rightarrow H_{v_{tan}}(s) = \frac{\delta V_{tan}(s)}{\delta V_c(s)} = \frac{1}{\frac{mL^2}{c}s + 1}$$

1.4 Determination of the Pendulum Length

The damping ratio ζ can be determined, using the logarithmic decrement. In this experiment, the maximal amplitude of the angle θ for two consecutive periods are measured. This is shown in Figure 3, where T stands for the period of the oscillation. The logarithmic decrement δ is then defined as [3]:

$$\delta = ln\left(\frac{\theta(t)}{\theta(t+T)}\right) = \frac{2\pi\zeta}{\sqrt{1-\zeta^2}} \tag{15}$$

Where $\theta(t)$ and $\theta(t+T)$ are both the values of the maximal angle in their period. From Equation 15, ζ can be derived:

$$\zeta = \frac{\delta}{\sqrt{(2\pi)^2 + \delta^2}} \tag{16}$$

By measuring the period of the oscillations, the distance L from the rotating point to the centre of gravity can be calculated. since the pendulum has two bolts detached at the end of it, the centre of gravity will be located close to the end, but the distributed mass of the pendulum will cause the calculated length L to be smaller than the measured length from the rotating point to the end of the pendulum L_m.

From the measured period, we can derive the measured (damped) pulsation, which is an estimate for the real pulsation.

$$\omega_d = \frac{2\pi}{T} = \omega_n\sqrt{1-\zeta^2} \tag{17}$$

From Equation 17, the natural pulastion ω_n can be derived. As $\omega_n = \sqrt{\frac{g}{L}}$, L can be found as:

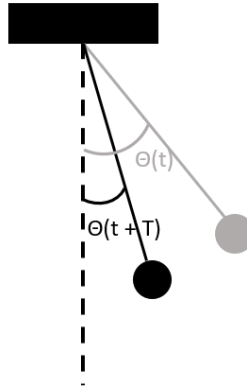$$L = \frac{g}{\omega_n^2} = \frac{g(1-\zeta^2)}{\omega_d^2} \tag{18}$$

Figure 3: Measured values for the experiment to determine ζ

The numerical values are: $T = 0.71s$, $L = 0.1258m$, $\zeta = 0.0327[-]$. As expected, the measured length $L_m = 0.151m$ is larger than de calculated length L. If the damping is neglected, the measured pulsation ω_d is equal to the natural pulsation ω_n and the length can be calculated as $L' = \frac{g}{\omega_d^2} = 0.1259m$.

The damping coefficient c is related to the damping ratio ζ via Equation 19. As the pendulum mass is unknown, the moment of inertia J is unknown and c can not be calculated.

$$\zeta = \frac{c}{c_{crit}} = \frac{c}{2J\omega_n} \tag{19}$$

Important note: For the remainder of this report, the damping will be neglected.

1.5 Discretization

Linear model

To discretize the linear model, the forward Euler method is used:

$$\delta\dot{\xi} = \frac{\delta\xi[k+1] - \delta\xi[k]}{T_s} \tag{20}$$

Filling in Equation 20 in Equation 8 yields the following equation:

$$\delta\xi[k+1] = (\mathbf{I} + T_s\mathbf{F})\delta\xi[k] + T_s\mathbf{G}\delta v_c[k] \tag{21}$$

Which can be translated into the following discretized, linear state-space model (where the damping is neglected, $c = 0$):

$$\delta\xi[k+1] = \begin{bmatrix} 1 & 0 & 0 \\ 0 & 1 & \frac{T_s}{L} \\ 0 & -gT_s & 1 \end{bmatrix} \delta\xi[k] + \begin{bmatrix} T_s \\ \frac{-T_s}{L} \\ 0 \end{bmatrix} v_c[k]$$

$$\begin{bmatrix} x[k] \\ \theta[k] \end{bmatrix} = \begin{bmatrix} 1 & 0 & 0 \\ 0 & 1 & 0 \end{bmatrix} \xi[k] + 0 \cdot v_c[k] \tag{22}$$

Non-linear model

To discretize the non-linear model, the forward Euler method is used as well:

$$\dot{\xi} = \frac{\xi[k+1] - \xi[k]}{T_s} \tag{23}$$

By filling in Equation 23 in Equation 6 the following equation can be derived:

$$\xi[k+1] = T_s\mathbf{f}(\xi[k], v_c[k]) + \xi[k] \tag{24}$$

By neglecting the damping of the system, following discretized, nonlinear state-space model can be found:

$$\xi[k+1] = \begin{bmatrix} T_s v_c[k] + x[k] \\ T_s \cdot \frac{v_{tan}[k] - v_c[k]\cos(\theta[k])}{L} + \theta[k] \\ T_s\left(-g\sin(\theta[k]) - v_c[k]\sin(\theta[k])\frac{v_{tan}[k] - v_c[k]\cos(\theta[k])}{L}\right) + v_{tan}[k] \end{bmatrix} \tag{25}$$

$$\begin{bmatrix} x[k] \\ \theta[k] \end{bmatrix} = \begin{bmatrix} 1 & 0 & 0 \\ 0 & 1 & 0 \end{bmatrix} \xi[k] + 0 \cdot v_c[k] \tag{26}$$

2 Design and implementation of a linear Kalman filter

The linearized measurement equation is given by Equation 26. For the matrices Q, R and $\hat{P}_{0|0}$, the following numerical values are used:

$$\mathbf{R} = \begin{bmatrix} 2.7878 \cdot 10^{-9} & 0 \\ 0 & 9.4124 \cdot 10^{-6} \end{bmatrix} \begin{bmatrix} \text{m}^2 \\ \text{rad}^2 \end{bmatrix} \tag{27}$$

$$\mathbf{Q} = \begin{bmatrix} 2.7878 \cdot 10^{-8} & 0 & 0 \\ 0 & 9.4124 \cdot 10^{-8} & 0 \\ 0 & 0 & 10^{-4} \end{bmatrix} \begin{bmatrix} \text{m}^2 \\ \text{rad}^2 \\ \left(\frac{\text{m}}{\text{s}}\right)^2 \end{bmatrix} \tag{28}$$

$$\hat{\mathbf{P}}_{0|0} = \begin{bmatrix} 10^{-6} & 0 & 0 \\ 0 & 2.3511 \cdot 10^{-6} & 0 \\ 0 & 0 & 10^{-6} \end{bmatrix} \begin{bmatrix} \text{m}^2 \\ \text{rad}^2 \\ \left(\frac{\text{m}}{\text{s}}\right)^2 \end{bmatrix} \tag{29}$$

The value of $\mathbf{R}_{11} = R_x$ is determined by estimating the resolution of the wheel encoder experimentally. To this extent, the wheel is manually rotated as little as possible. The position values of the motors obtained using `getPositionMotorA()` are compared before and after this rotation. In this report, the difference in positions is 0.0032 m. Dividing this difference by 2 yields the maximum possible deviation of the position x, after multiplication by the radius of the wheels. This last operation is because the previously mentioned formula returns the position in radians, while x is expressed in meters. Finally, the measurement noise covariance is given as the square of this last calculated value.

$\mathbf{R}_{22} = R_\theta$ is also determined using the resolution of the pendulum encoder. For this sensor, the resolution is already given and is equal to 1024 steps per revolution. This means that the pendulum angle can be determined with an accuracy of $0.5 \cdot \frac{2\pi}{1024}$ radians. Again, taking the square of this value yields the measurement noise covariance for the pendulum angle θ.

For the values of Q_x and Q_θ, experiments with varying Q are conducted, of which the best ones yield the values given in (28). The best experiments are those that lead to the estimated states being the closest to reality. This way, Q_x is set to $10 \cdot R_x$, while Q_θ is set to $0.01 \cdot R_\theta$. Lastly, $Q_{v_{tan}}$ is taken in the order of the square root of Q_x and Q_θ, because v_{tan} involves a derivative.

Next, for $\hat{P}_{0|0,\theta}$, the following experiment is conducted: the pendulum is manually set so that one thinks that $\theta = 0$. Then, the measured angle θ shows how much one deviates from $\theta = 0$. This is repeated multiple times. The largest value of the measured angle over all the experiments is then taken as the maximum deviation when one wants to place the pendulum at $\theta = 0$. In this report, this value is taken to be 0.0046 rad. Following the *68-95-99.7 rule*[1] then leads to $\hat{P}_{0|0,\theta} = \left(\frac{0.0046}{3}\right)^2 = 2.3511 \cdot 10^{-6}$ rad^2. Lastly, $\hat{P}_{0|0,x}$ and $\hat{P}_{0|0,v_{tan}}$ are taken in the same order, leading to a value of 10^{-6}.

With wheel and pendulum encoder

Now, a trapezoidal velocity profile is applied as input. Figure 4 then depicts the evolution of every state in time together with its 95% confidence interval. As the states x and θ can be measured using respectively the wheel encoders and the pendulum encoder, these measurements are also plotted with their 95% confidence interval. On the full-scale plots, it is hard to see these intervals for x and θ, so a close-up of these states are likewise shown.

For x, one can observe that the confidence interval of the estimate is larger than the interval of the measurement. Subsequently, the uncertainty of the estimated state is larger than the uncertainty of the measured state. This is not in accordance with the Kalman filter principles, as using it only is valuable whenever the obtained estimate is better than the measurement, which matches with the confidence interval of the model being lower than the interval of the measurement. Conclusion: using a Kalman filer for the state x produces worse results.

For θ, both confidence intervals almost overlap. Again, this does not match the expectations of the Kalman filter. However now, using it produces roughly equally good results.

Lastly, for v_{tan}, Kalman filtering is per definition useful, as this state cannot be measured directly.

Without wheel encoder

The experiments are repeated, but now without using the wheel encoder. I.e. the state x is not measured anymore, solely θ is measured. Consequently, the measurement equation changes to:

$$\theta[k] = \begin{bmatrix} 0 & 1 & 0 \end{bmatrix} \xi[k] + 0 \cdot v_c[k] \tag{30}$$

Figure 5 depicts again the evolution of every state in time together with its 95% confidence interval. Now, the measured response can only be plotted for the state θ, together with its 95% confidence interval. It is
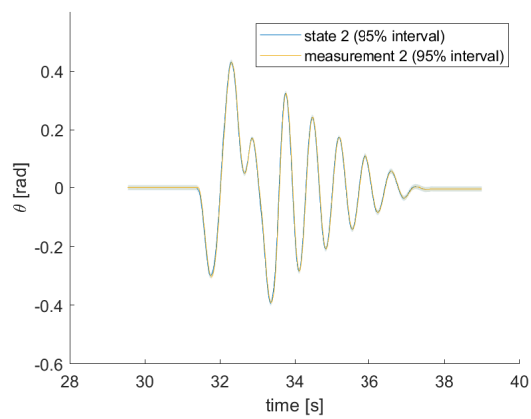
---

[1] "In statistics, the 68–95–99.7 rule, also known as the empirical rule, is a shorthand used to remember the percentage of values that lie within an interval estimate in a normal distribution: 68%, 95%, and 99.7% of the values lie within one, two, and three standard deviations of the mean, respectively." [1]
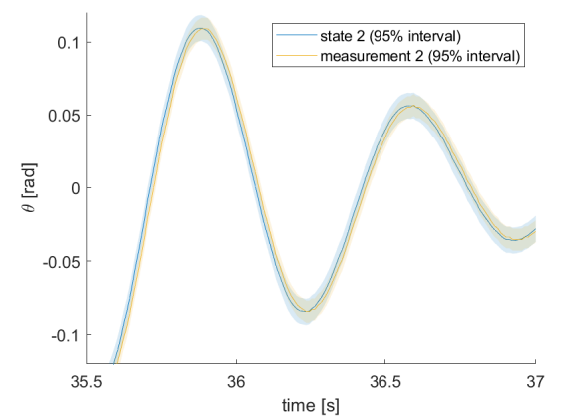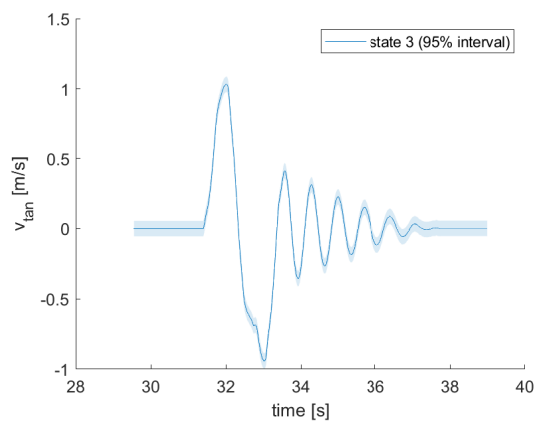
(a) x

(b) x (close up)

(c) θ
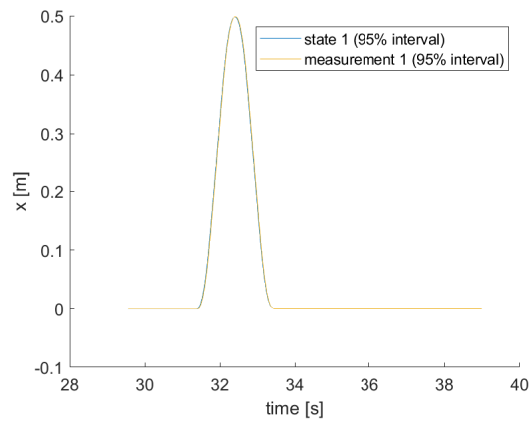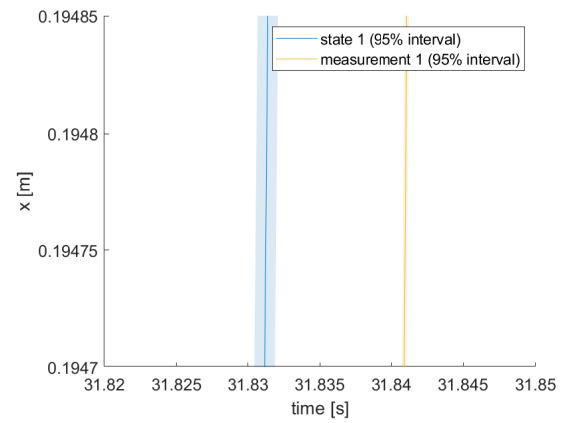
(d) θ (close up)

(e) v_{tan}

Figure 4: Yeet

obvious that the uncertainty for the estimation of x has increased a lot. This is because normally, during the correction step of the Kalman filter, the estimated value is adjusted with a factor of the Kalman gain L_k:

$$\hat{x}_{k+1|k+1} = \hat{x}_{k+1|k} + L_{k+1} \cdot (y[k+1] - \hat{y}[k+1]) \tag{31}$$

Because there is no measurement for x, the correction step will never adjust the a priori state estimate. Consequently, the uncertainty of the state estimate is constantly increased, as can also be confirmed by the diverging confidence interval in Figure 5b.

3 Design and implementation of an extended Kalman filter

3.1 Nonlinear measurement equation

As is already written down in the nonlinear state-space model Equations 7, the measurement equation based on the nonlinear system equations is actually a linear equation. This is caused by the fact that the two outputs x and θ are two states. The measurement equation based on the nonlinear system equations can be written as:

$$\mathbf{y} = \begin{bmatrix} x \\ \theta \end{bmatrix} = \mathbf{g}(\xi, v_c) = \begin{bmatrix} 1 & 0 & 0 \\ 0 & 1 & 0 \end{bmatrix} \xi + 0 \cdot v_c \tag{32}$$

3.2 Jacobian of the state and measurement equation

The Jacobian matrix of the state equation and the Jacobian matrix of the measurement equation can be found by taking the derivative of the functions $\mathbf{f}$ (Equation 25) and $\mathbf{g}$ (Equation 32) to the state vector ξ

$$\mathbf{A} = \frac{\partial \mathbf{f}}{\partial \xi}$$
$$\mathbf{C} = \frac{\partial \mathbf{g}}{\partial \xi} \tag{33}$$

Unlike the linear Kalman filter, the extended Kalman filter uses discretized jacobian matrices evaluated in the current state estimate and not in the equilibrium state. Using Equations 33, following expressions can be derived for the discrete time jacobians, starting from nonlinear, discrete state-space model 25. Damping is neglected:

$$\mathbf{A} = \begin{bmatrix} 1 & 0 & 0 \\ 0 & 1 + T_s \frac{v_c \sin(\theta)}{L} & \frac{T_s}{L} \\ 0 & T_s\left(-g\cos(\theta) - \frac{v_{tan} - v_c \cos(\theta)}{L} \cdot v_c \cos(\theta) - \frac{(v_c \sin(\theta))^2}{L} \right) & 1 + T_s \frac{-v_c \sin(\theta)}{L} \end{bmatrix}$$
$$\mathbf{C} = \begin{bmatrix} 1 & 0 & 0 \\ 0 & 1 & 0 \end{bmatrix} \tag{34}$$

## 3.3 Implementation of the extended Kalman filter

Since the linearization of the model has no influence on the measurement noise covariance or the covariance of the initial state estimation errors, the values for $\mathbf{R}$ and $\hat{\mathbf{P}}_{0|0}$ for the extended Kalman filter are taken equal to those used in the linear Kalman filter (see Equations VERWIJZEN NAAR VROEGERE MATRICES). As the nonlinear model is used for the extended Kalman filter, the model should be more precise and thus the proces noise should be lower. For this reason $\mathbf{Q}$ is taken one order of magnitude smaller than the $\mathbf{Q}$ used in the linear Kalman filter.

$$\mathbf{Q} = \begin{bmatrix} 2.7878 \cdot 10^{-9} & 0 & 0 \\ 0 & 2.3511 \cdot 10^{-9} & 0 \\ 0 & 0 & 10^{-5} \end{bmatrix} \tag{35}$$
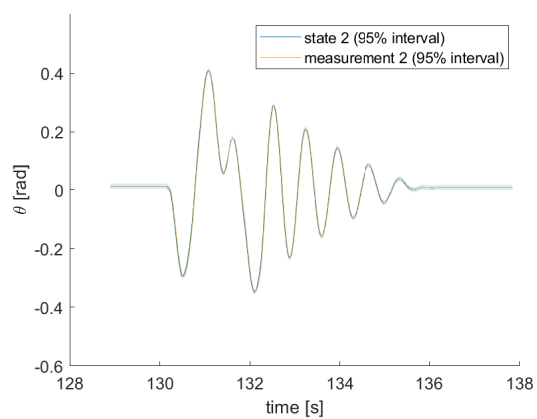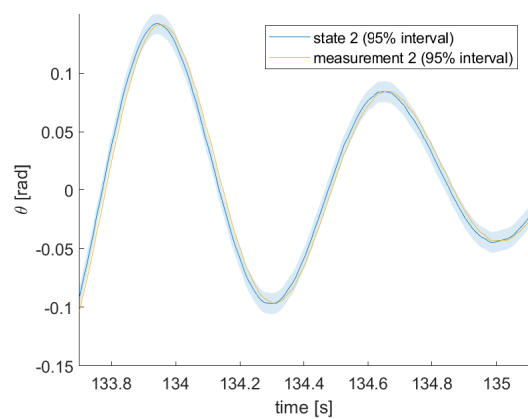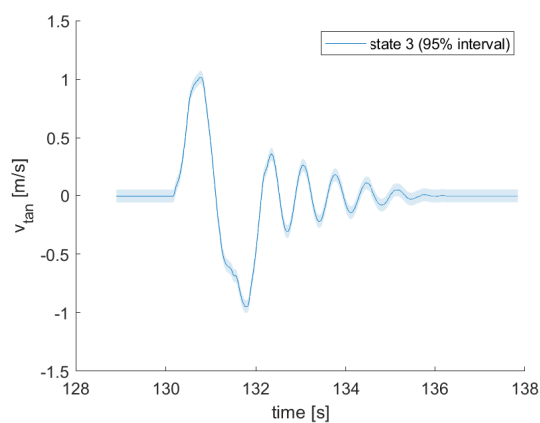
GRAFIEKEN + UITLEG

(a) x

(b) x (close up)

(c) θ
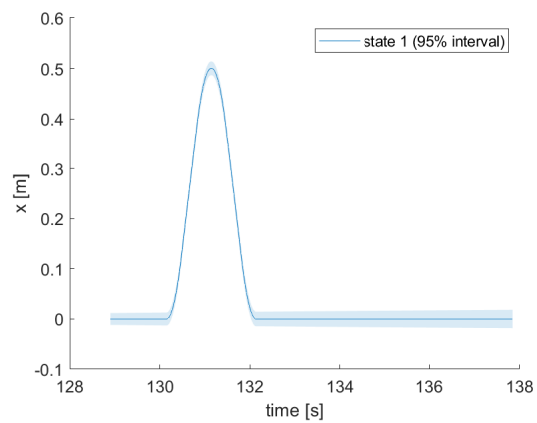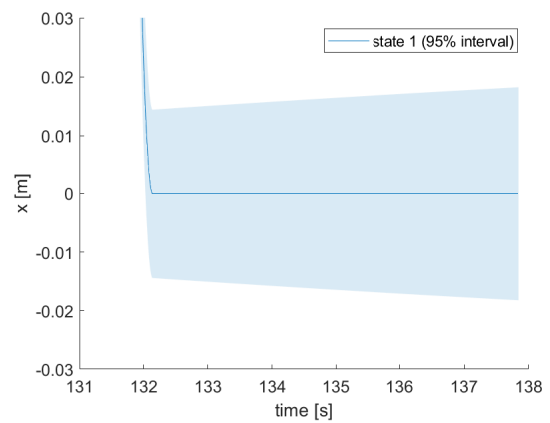
(d) θ (close up)

(e) v_{tan}

Figure 5: Yeet

4 Design and implementation of a state feedback controller based on the linearized model

4.1 Design of a linear quadratic regulator

The objective of the LQR is to find the control input $v_c[k]$ that moves the system states $\xi \neq 0$ to $\mathbf{0}$, in a way the performance criterion $\mathcal{J}$ is minimized. This means a tradeoff has to be made between performane $\mathcal{J}_p$, the speed with which the states go to zero (or a desired state), and the controll effort $\mathcal{J}_c$. The criterion is given in Equation 36.

$$\mathcal{J} = \mathcal{J}_p + \mathcal{J}_c = \sum_{k=0}^{\infty} \xi[k]^T \mathbf{Q} \xi[k] + v_c[k] R v_c[k] \tag{36}$$

The matrix $\mathbf{Q}$ and the value R are design parameters. These values determine which part of the tradeoff is most important in this particular design: performance or control effort. The tuning of the parameters and thus the design of the LQR itself is done in Section 4.3.

4.2 Design of a feedforward gain

The blockdiagram of the system with feedforward compensation can be found in Figure 6.
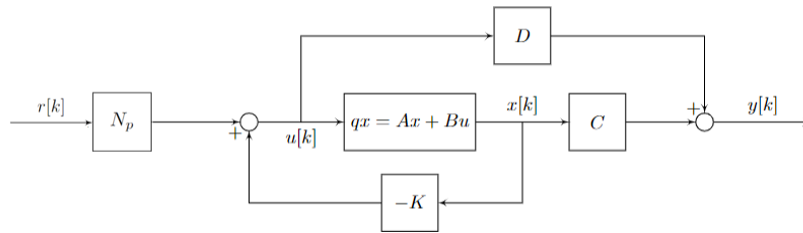

Figure 6: Blockdiagram of the system with feedforward compensation

The feedforward gain N_p is calculated such that the steady-state error equals zero for a step reference in desired position, which is denoted with $r[k]$. The pendulum mass position can be written as:

$$x_p = x + L \cdot \sin(\theta) = x + L \cdot \theta \tag{37}$$

x_p is thus a linear combination of the two outputs of the linear system. The total transfer function $\mathbf{H}(z)$ of the system is thus a vector containing 2 transfer functions: $H_x(z) = \frac{X(z)}{V_c(z)}$ and $\frac{\Theta(z)}{V_c(z)}$. The pendulum mass position can be calculated starting from a given v_c as follows:

$$X_p(z) = (H_x(z) + L H_\theta(z)) V_c(z) \tag{38}$$

Following the reasoning on C9, slide 54 of the slides of the course Control Theory [5], the expression for N_p to obtain a zero steady state error is: NOG HELEMAAL UITWERKEN OF GWN VERWIJZEN NAAR SLIDE?

$$N_p = \frac{1}{(H_x(1) + L H_\theta(1))} \tag{39}$$

To be able to use $H_x(z)$ and $H_\theta(z)$, $\mathbf{H}(z)$ has to be calculated. This can be done using Equation 40.

$$\mathbf{H}(z) = \mathbf{C}(z\mathbf{I} - \mathbf{A} + \mathbf{B}\mathbf{K})^{-1}\mathbf{B} \tag{40}$$

The matrices $\mathbf{A}$,$\mathbf{B}$ and $\mathbf{C}$ can be found in Equation 22. When the feedback gain $\mathbf{K}$ is calculated in Section 4.3, it will become possible to calculate $\mathbf{H}(z)$ thus also N_p.

4.3 Implementation of the controller

References

[1] 68–95–99.7 rule. `https://en.wikipedia.org/wiki/68-95-99.7_rule`, 2021. Last accessed December 23rd 2021.

[2] Aurelio Arenas. The use of a nintendo wii remote control in physics experiments. `https://www.researchgate.net/publication/258272199_The_use_of_a_Nintendo_Wii_remote_control_in_physics_experiments`, 2013. Accessed December 17th 2021.

[3] W. Desmet. *Mechanische trillingen - Slides*. Cursusdienst VTK, 2021.

[4] Michel Levis. Common and not zo common pendulum configurations. `https://www.quanser.com/blog/common-and-not-so-common-pendulum-configurations/`, 2019. Accessed December 17th 2021.

[5] Swevers J. Pipeleers G. *Control Theory - Handouts*. Cursusdienst VTK, 2021.